COMMENTS ON THE OBSERVABILITY OF CORONAL VARIATIONS

L. GOLUB[1], T. W. HARTQUIST[2], and A. C. QUILLEN[1,3]

(Received 6 January, 1989; in revised form 30 January, 1989)

Abstract. We discuss the observable variability of spectral lines in the soft X-ray and XUV region. Rapid variability of coronal emission, both in flaring and non-flaring structures has been reported and is particularly prominent when high spatial resolution is available. Examination of the ionization and recombination time-scales for the formation and removal of ions with prominent solar emission lines shows that, even though ionization equilibrium generally prevails, the observable variability time-scales are often limited by these atomic processes, independent of the physical process which is causing the change in the solar atmosphere. Rapid heating can lead to an initial freezing-in of abundances of some ions; observations of at least one low- and one high-excitation line from such an ion would permit studies of the time evolution of the emission measure and temperature. In a very limited number of cases, rapid cooling leads to freezing-in of the abundance of an ion and observations of a low-excitation line of this ion will not yield accurate information about the thermal evolution. Thus, future observations of Mg X 609 Å should be augmented by simultaneous observation at another wavelength, such as 63 Å. In addition, with the ability to produce images in isolated spectral lines it becomes possible to select those for which rapid variability is observable, such as O VII, rather than lines which were selected on the basis of previous hardware constraints, such as O VIII.

1. Introduction

Techniques for the fabrication of thin film multilayer coatings capable of reflecting X-rays have progressed rapidly in recent years (for a review, see Barbee, 1985). It has now become possible to design and construct astronomical instruments which employ multilayer coated optical elements and operate at normal incidence at wavelengths in the region from 44 to ~ 304 Å (Golub *et al.*, 1985; Underwood *et al.*, 1987; Walker *et al.*, 1989). With the development of normal incidence X-ray and XUV telescopes, high spatial (~ 0.1 arc sec) resolution observations of individual spectral lines emitted by the solar coronal and transition region plasmas are now possible. Designs which include dispersive elements are also being developed, as are designs using multilayers at grazing angles permitting their use at shorter wavelengths (see the review by Catura and Golub, 1988).

Because this new technology is available and is beginning to be used in solar observations, the present time is opportune for addressing questions related to the observability of temporal variations in individual emission lines caused by the dynamical and physical evolution of the emitting regions. In the following, we will identify previously detected solar emission lines which are suitable for the study of variability in plasmas with the specific combinations of pressure, temperature and spatial scales which are found in the

[1] Smithsonian Astrophysical Observatory, Cambridge, MA, U.S.A.
[2] Max-Plank-Institut für Physik und Astrophysik, D-8046 Garching, F.R.G.
[3] Astronomy Dept., California Inst. of Tech., Pasadena, CA, U.S.A.

Solar Physics **122** (1989) 245–261.
© 1989 *by Kluwer Academic Publishers. Printed in Belgium.*

solar atmosphere, and then we will explore the types of variability which can be observed in each of these lines.

Rapid non-flare variability of coronal emission from individual loop structures seen in Fe XV at 284 Å was reported by Sheeley and Golub (1978). These data had 2 arc sec resolution, which permitted the individual loops in active regions to be resolved, whereas simultaneous observations in broadband X-rays, which had somewhat lower resolution, did not resolve these structures. Short time-scale variability was not observed in X-rays and this lack of variability was interpreted as due to an averaging over the emission from several loops in the active region (Nolte, Solodyna, and Gerassimenko, 1979), which smooths out the variability of the individual structures.

These observations show that rapid variability does occur within active regions, and that spatial resolution of better than 2 arc sec is needed for studies of these structures. However, our present study shows that the interpretation given by Nolte, Solodyna, and Gerassimenko, for the lack of variability in X-rays may not be correct. The X-ray emission which they observed was dominated by Fe XVII in the thin Be filter, or by a combination of Fe XVII, O VII, and O VIII in the polypropylene filter, with the latter possibly dominating. As we discuss in Section 3.3, the time-scale for variability of the emission in O VIII at the temperature and density appropriate to typical coronal regions is several minutes. This is equal to or greater than the time-scales observed in Fe XV, for which ionization equilibrium is established in a few tens of seconds.

Thus, the failure to observe variability in X-rays may have been an artifact of the instrumentation used, rather than anything intrinsic to the active region under study. Instruments which can provide imaging in a single spectral line are in some ways more susceptible to this problem, because an incorrect choice cannot be compensated by another line in the passband. For the study described above, the ability to choose O VII rather than O VIII would have provided diagnostics with 0.1 s time resolution.

Observations in more than one spectral line are needed in order to distinguish between temperature and density variations, since the emission from any single line by itself will yield information that mixes emission measure and temperature. For example, it is possible to observe temporal variability more rapid than the ionization times if the emission measure changes rapidly.

High spatial and moderate spectral resolution observations may reveal not only the variability of individual loop structures, but also the possible substructure within coronal loops. In coronal heating models based on reconnection and current dissipation (e.g., Kuperus, Ionson, and Spicer, 1981), the primary heating is confined to very thin current sheaths which may heat the loops in either a steady or intermittent fashion. In either case, the loops should exhibit small scale thermal substructure with associated variability.

Martens, van den Oord, and Hoyng (1985) have reported observations of the corona using the HXIS instrument on the SMM satellite; their interpretation of the data is that '0.1% of the loop is filled with a plasma with a temperature of about 10^7 K and a density of 10^{11} cm^{-3}'. The temperature and density in the remaining 99.9% of the loop volume are 'much smaller'. Observations such as these offer indirect evidence that loop substructure is present, and it is likely to be highly variable on short time-scales.

The aim of this paper is to discuss the appropriateness of specific XUV and soft X-ray emission lines for studies of coronal variability. Among our major conclusions are the realization that, for many of the typical regions found in the solar outer atmosphere, the observable time-scales for variability are determined by the ionization and recombination time-scales of the plasma rather than by the inherent nature of the physical process causing the variability. Moreover, we find that cases exist in which conductive cooling dominates and that in some of these cases the 'freezing-in' of the ionization structure of a species affects the emissivity. If the particular line being observed originates from a lowly excited level then the freezing-in will lead to the line's strength varying slowly compared to the cooling time. On the other hand, we show that diagnostics exist which can be used to determine whether or not conductive cooling is important in a particular event.

The organization of this paper is as follows: in Section 2 we list the lines which are most likely to be used in future observations and describe their applicability in diagnostic studies of coronal emission under the variety of conditions encountered on the Sun. In Section 3 we consider the ways in which the time-scale for electron impact production of particular species affects the utility of those species for diagnosing changes in the coronal plasma; in the same section, we also treat cooling plasmas.

2. Selection of Lines

The X-ray and XUV emission lines which we have studied were selected on the basis of several criteria:

(i) We chose the strongest lines in the solar spectrum, based both on theoretical calculations and on observations which ensure that the line is actually present.

(ii) We arbitrarily chose to limit our search to the range of wavelengths for which multilayer optics might be used. We take this range to be ~ 15 Å at the short end and 304 Å at the other end.

(iii) Specific consideration was given to selecting those lines which would provide unambiguous diagnostics over the full range of temperatures from the chromosphere through flare levels (i.e., 10^4 to $10^{7.5}$ K).

The results of this search are not entirely satisfactory, in that the combination of technological difficulties and placement in the spectrum of the most interesting lines overlap in unfortunate ways. The results of the search can be summarized by the following three groupings:

(I) 15–44 Å: this region contains the emission lines which for pure coronal imaging and diagnostics might be considered the most desireable, viz., Fe XVII, O VII, O VIII, C VI, etc. However, it does not seem possible at the present time to manufacture multilayers which work with any reasonable efficiency at normal incidence at these wavelengths. Grazing incidence (~ 10–$20°$) applications are possible, but these to some extent remove the enormous advantage in terms of spatial resolution which is achieved by going to normal incidence.

(II) 44–170 Å: in this region production of high performance multilayers becomes

feasible, especially longward of 60 Å. However, the coronal emission lines in this region are comparatively weak and construction of a practical observing instrument is difficult because of the low intensity levels.

(III) 171–304 Å: strong emission lines with important diagnostic value are found in this spectral region and high reflectivity multilayers are easily manufactured at these wavelengths. However, the spectrum is relatively crowded with strong emission lines and, because only a few layers are needed in order to achieve high reflectivity in the multilayer it is quite difficult to obtain a narrow band coating. Thus, the data will in general be contaminated by a mixture of different lines all imaged on top of each other. In principle this problem can be overcome by introducing a dispersive element into the optical system, or by very clever design of the multilayer; neither of these two solutions has yet been demonstrated in practice, however.

The lines which we have chosen are listed in Table Ia. Sources examined in the selection process include, among others: Freeman and Jones (1970), Manson (1972), Malinovsky and Heroux (1973), Doschek and Cowan (1984), and Acton, Bruner, and Brown (1985). The decision as to which lines will be most useful for coronal studies depends to a large extent upon the plasma conditions which are prevalent in the atmospheric feature (or event) of interest. There is no single best answer to this question, since typical features or events usually have a connection to the photosphere or below, thus encompassing temperatures from ~ 5000 K to 10^6 or as high as 10^8 K in extreme cases. However, a useful method of characterizing the study is to examine the coronal temperature, pressure, and geometry, after which the lower temperature portions of the atmosphere are to some extent specified.

A simplified tabulation of typical plasma parameters is provided in Table Ib. It should be understood that these are only typical values, listed in order to show the general range observed. In the following discussion we use this table as a starting point for an examination of the spectral lines which will be most useful for studying each of these coronal phenomena.

The solar atmosphere is inherently complicated and atmospheric studies typically will require high resolution two-dimensional imaging and some type of spectroscopy. Structures with sizes ranging from the resolution limit (~ 200 km) to several solar radii ($> 10^6$ km) are seen and major changes in these structures occur on time-scales from milliseconds during the rise phase of a flare (bursts), to tens of minutes for flares (gradual phase), to months for the evolution of the large-scale structure. It is not likely that a single instrument can be designed which will diagnose the full range of conditions which are present on the Sun, and in fact the usual answer is to provide a complement of instruments which together form a solar observatory.

The range of wavelengths over which multilayer coated optics can be used helps in deciding which subset of the overall problem will be attacked. In the 'multilayer regime' the emission lines listed in Table Ia cover a temperature range which includes the transition region and the corona, as well as thermal flare plasma. Thus our discussion centers around the type of problem typically treated by a grazing incidence X-ray telescope, with the addition of some of the lower temperature regions usually treated by

TABLE Ia

Soft X-ray and XUV lines included in this study

Species	Wavelength (Å)	$\log(T_{max})$
Fe XVII	16.78	6.6
	17.05	
	17.10	
O VIII	18.97	6.5
O VII	21.60	6.3
	21.81	
	22.10	
C VI	33.74	6.1
Si XII	45.52	6.3
	45.68	
Si XI	49.22	6.2
Mg X	57.9	6.1
Si VIII	61.0	6.0
Fe XVI	62.88	6.4
	63.71	
Mg X	63.15	6.1
	63.29	
Ne VIII	88.08	5.8
Fe XVIII	93.93	6.8
Ne VIII	98.26	5.8
Ne VII	115.52	5.7
	116.69	
Fe XXII	116.29	7.1
	117.17	
Fe IX	171.07	6.0
O V	172.17	5.4
O VI	172.94	5.5
	173.08	
Fe X	174.53	6.1
	177.24	
Fe XI	180.41	6.2
	182.17	
	188.22	
O VI	183.95	5.5
	184.13	
Fe XXIV	192.03	7.3
Fe XII	192.40	6.2
	193.52	
	195.13	
Fe XIV	211.32	6.2
	274.24	
He II	256.37	4.6
Fe XV	284.16	6.3
He II	303.79	4.6
Si XI	303.33	6.2

TABLE Ib

Typical plasma parameters for solar atmospheric features

Target	Size ($\times 10^9$ cm)	N_e (cm^{-3})	T (10^6 K)	Lines
Quiet corona	20	$1-3 \times 10^8$	1.6	O VII, C VI, Mg X, Fe XI, Fe XII
Extended corona	70	10^7	1.4	Fe X, Mg X, Ne VII
Polar plumes	50	10^8	1.3	Mg X, Fe X, Ne VIII
Active region	5–20	10^9–10^{10}	2–3	O VIII, Fe XVII, Fe XVI, Fe XV
Loop microstructure	<1	10^{11}	10	Fe XVIII, Fe XXII, Fe XXIV
X-ray bright point	0.2–2	5×10^9	1.8	O VII, Si XII, Fe XIV
Compact flare	2–3	10^{11}	20	Fe XXII, Fe XXIV
Two-ribbon flare	10	2×10^{10}	10	Fe XVIII, Fe XXII, He II

an XUV or UV spectroheliograph, such as the S-082A instrument on *Skylab*. The spectral lines which are of interest for the regions or events listed in Table Ib are obtained from Table Ia by comparing the temperature, emission measure and variability time-scales; results are listed in Table Ib in the last column.

3. Response of the Plasma to Rapid Heating or Cooling

3.1. General principles

Shapiro and Moore (1977) and Shapiro and Knight (1978) have pointed out that the plasma properties in solar flare regions vary on time-scales which are short relative to the time-scales on which the ionization structure attains equilibrium. It is feasible to perform detailed calculations of the nonequilibrium ionization structure and emissivity for a small number of specific combinations of plasma conditions and thermal histories as did Shapiro and Moore (1977).

However, coronal events display a wide variety of properties and in practice more general considerations, of utility for the study of any given coronal plasma, are required. For instance, Shapiro and Knight (1978) discussed the initial increases in the strengths of high excitation lines (i.e., those for which the excitation energy is comparable to or higher than kT_o, where T_o is the original temperature), and the subsequent decreases due to collisionally incuded ionization. They argued that the observed enhancement of a single properly-chosen high excitation line can be used to determine the increase in temperature, while the subsequent decay of the line strength yields information about the density of the plasma. They envisaged the ionization remaining frozen-in initially with its preheating structure and the increase in a line's emissivity being due to the temperature increase; the contribution to the line strength's increase due to stripping of less ionized species was ignored. The subsequent decrease in the line's emissivity occurs at the density-dependent ionization rate.

In fact, a plasma in which both the density and temperature have grown rapidly can be studied best by comparing the temporal evolution of the strength of high-excitation

line and a low-excitation line. The increase in the strength of the low-excitation line will be due primarily to the increase in the emission measure ($n_e^2 V$, where V is the volume) since the temperature dependence of an electron impact excitation rate generally is fairly weak when the energy of the impacting electron is much greater than the excitation energy. The increase of the strength of the high-excitation line will result from both the rise in the emission measure and from the rise of the temperature, the latter usually leading to a rapid growth in the collisional excitation rate of a high-excitation line.

In structures in which the conductive cooling is very strong, the cooling may also occur on a time-scale which is short compared to that required for electron impact induced ionization to produce species which normally would be abundant in an equilibrium situation. The absence of emission features which would be prominent in an equilibrium plasma at its temperature maximum may lead one to underestimate the maximum temperature attained. Clearly, the variability of the plasma properties cannot be observed in lines of those species which cannot be ionized on time-scales shorter than the evolutionary time-scales of the plasma.

Simultaneous observations of a high-excitation line and of a low-excitation line are also useful for diagnostic studies of a plasma which is cooling rapidly. In plasma which is cooling due to rapid conductive heat loss, the ionization states may be frozen in with a structure similar to that which obtains in a high temperature equilibrium plasma. If freezing in does occur, low excitation lines emitted from highly ionized species will continue to be strong and would generally increase in strength as a function of time if the plasma pressure remains constant during the cooling phase. However, the strengths of the corresponding high-excitation lines would decrease relatively rapidly with plasma temperature. From simultaneous measurements of a low-excitation line and a high-excitation line of frozen in highly ionized species, the temperature and emission measure evolutions could be derived. As a practical matter, it is preferable if the two lines are of the same ion, in order to keep the analysis as uncomplicated as possible.

An example of this effect is given in Figure 1, which compares the 52.9 Å emission of Fe XV to the 284 Å emission, using values taken from Mewe, Gronenschild, and van den Oord (1985). The emissivity curves for the ion are identical, but dividing by the fractional abundance f for the respective lines in question introduces a major change, as shown by the upper curves in the figure. Thus, if material which is initially at a temperature of $\log T = 6.3$ cools rapidly to a temperature of, e.g., $\log T = 6.0$, then the decrease in strength of Fe XV at 284 Å can be as much as a factor of three less than that of the 52.9 Å line.

3.2. Variability time-scales for line emission

In Section 2, we identified lines which have been detected previously and which are prime candidates for use in higher resolution studies of the corona. So that we can identify which lines are likely to be of diagnostic value, we have calculated the ionization and recombination time-scales of various ions at different temperatures for plasma in which the pressure $n_e T$ is arbitrarily taken to be equal to the value 3×10^{15} cm^{-3} K, where n_e and T are the electron density and temperature. Data for the calculation of

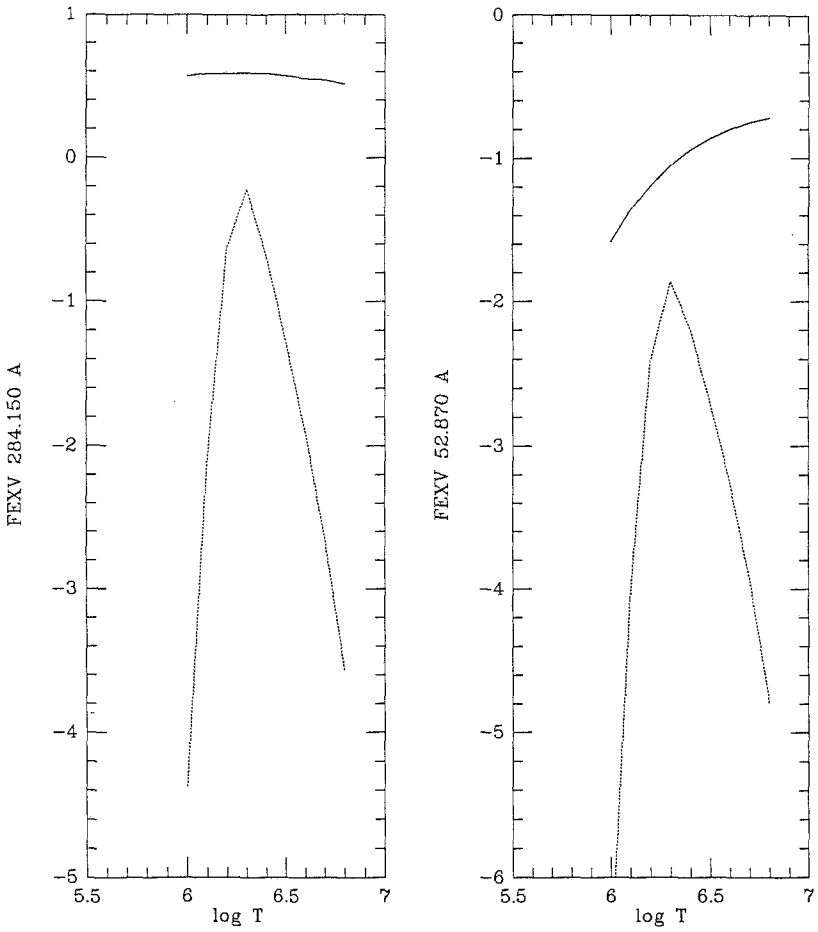

Fig. 1. Comparison of the emissivity of a low- and high-excitation line of the species Fe^{+14}. The upper curves show the emissivity divided by the fractional abundance for each line.

these time-scales come from the compilation by Arnaud and Rothenflug (1985, and references therein), primarily the papers of Woods, Shull, and Sarazin (1981) and of Shull and van Steenburg (1982). In general, the time-scales are inversely proportional to the pressure, but at high densities, dielectronic recombination may be suppressed.

The fraction, f, of an element that is in a given ionization stage in a low-density equilibrium plasma can be found in the paper by Arnaud and Rothenflug (1985). For several species, we give f and various ionization and recombination time-scales as a function of temperature in Table II. In addition to several ions which are especially prominent in the solar spectrum, the species C^{+5} and Fe^{+9} are included because they have lines which arise from states with very different excitation energies, making them useful as diagnostics when studying rapid heating events. The species Fe^{+17}, O^{+6}, and Mg^{+9} are abundant in equilibrium plasmas over a wide range of temperatures and are observable in at least two types of solar coronal regions (viz., Table II).

We calculate time-scales for four processes which can influence the appearance and

TABLE II

Ionization and recombination time-scales[a] as a function of temperature

$\log T$	t_{if}	t_{ir}	t_{rr}	t_{rf}	$-\log f$
			C VI		
5.7	7.8e3	2.1e5	1.6e2	86	1.7
5.8	1.4e3	2.4e4	2.2e2	1.3e2	0.9
5.9	3.5e2	4.2e3	2.6e2	1.9e2	0.4
6.0	1.2e2	1.1e3	2.7e2	2.9e2	0.2
6.1	56	4.0e2	2.7e2	4.3e2	0.4
6.2	31	1.8e2	2.8e2	6.5e2	0.7
6.3	20	1.0e2	3.1e2	9.9e2	1.0
6.4	15	65	3.7e2	1.5e3	1.4
6.5	12	48	4.7e2	2.3e3	1.7
			Fe X		
5.6	95	69	0.76	0.37	2.2
5.7	4.0	19	0.89	0.51	1.3
5.8	2.0	7.2	1.1	0.70	0.8
5.9	1.2	3.4	1.5	0.96	0.5
6.0	0.79	2.0	2.2	1.4	0.5
6.1	0.60	1.3	3.3	2.0	0.9
6.2	0.50	0.99	5.1	2.9	1.8
6.3	0.45	0.82	8.1	4.5	3.5
			Fe XVIII		
6.3	5.5e3	1.2e4	1.1e2	41	2.5
6.4	1.4e3	2.8e3	1.3e2	59	1.5
6.5	4.8e2	8.9e2	1.5e2	82	0.9
6.6	2.2e2	3.7e2	1.7e2	1.1e2	0.5
6.7	1.2e2	1.9e2	2.1e2	1.5e2	0.4
6.8	77	1.2e2	2.8e2	2.0e2	0.6
6.9	57	85	3.9e2	2.8e2	1.0
7.0	47	68	5.7e2	4.1e2	1.8
7.1	42	59	8.6e2	6.1e2	3.0
			Mg X		
5.8	2.7e2	1.3e3	13	58	3.0
5.9	90	3.7e2	21	88	1.5
6.0	39	1.4e2	34	1.3e2	0.7
6.1	21	70	56	2.0e2	0.7
6.2	13	41	92	3.1e2	0.9
6.3	9.6	28	1.5e2	4.6e2	1.2
6.4	7.8	22	2.5e2	6.3e2	1.5
6.5	6.8	18	4.1e2	7.8e2	1.7
6.6	6.5	17	6.7e2	9.0e2	1.8
6.7	6.5	16	1.1e3	1.0e3	1.9
6.8	6.9	17	1.8e3	1.2e3	2.2

Table II (continued)

$\log T$	t_{if}	t_{ir}	t_{rr}	t_{rf}	$-\log f$
			O VII		
5.3	5.6e–2	–	28	11	2.8
5.4	6.5e–2	–	42	17	1.1
5.5	7.7e–2	–	63	26	0.2
5.6	9.2e–2	6.e9	94	40	0.1
5.7	0.11	8.e7	1.4e2	61	0.0
5.8	0.14	2.7e6	2.1e2	93	0.0
5.9	0.16	1.8e5	3.0e3	1.4e2	0.0
6.0	0.20	2.3e4	4.0e3	2.0e2	0.0
6.1	0.24	4.5e3	4.4e3	2.7e2	0.0
6.2	0.29	1.3e3	4.3e3	3.3e2	0.1
6.3	0.36	4.8e2	4.2e3	3.9e2	0.3
6.4	0.44	2.3e2	4.4e3	4.6e2	0.6
6.5	0.54	1.3e2	5.0e3	5.7e2	1.1
6.6	0.68	88	6.2e3	7.4e2	1.7
			O VIII		
5.9	1.8e5	3.2e6	1.4e2	94	3.1
6.0	2.3e4	2.6e5	2.0e2	1.4e2	2.1
6.1	4.5e3	3.9e4	2.7e2	2.1e2	1.3
6.2	1.3e3	8.6e3	3.3e2	3.1e2	0.7
6.3	4.8e2	2.7e3	3.9e2	4.7e2	0.4
6.4	2.3e2	1.1e3	4.6e2	7.1e2	0.3
6.5	1.3e2	5.5e2	5.7e2	1.1e3	0.5
6.6	88	3.3e2	7.4e2	1.6e3	0.8
6.7	66	2.3e2	1.0e3	2.5e3	1.1
6.8	54	1.8e2	1.4e3	3.8e3	1.3
6.9	49	1.5e2	2.1e3	5.8e3	1.6
7.0	47	1.4e2	3.2e3	8.9e3	1.8
7.1	48	1.4e2	5.0e3	1.4e4	2.0
7.2	50	1.4e2	7.9e3	2.1e4	2.2
7.3	55	1.5e2	1.3e4	3.3e4	2.3

[a] All times are in seconds.

disappearance of a line. The time-scale, t_{if}, for the ionization of the next less ionized stage of an element and the time-scale, t_{ir}, for the ionization to the next more ionized stage of that element are shown. t_{rr} is the time-scale for the recombination to the next less highly ionized stage of the element and t_{rf} is the time-scale for the recombination of the next more highly ionized stage of the element. This nomenclature is defined schematically in Figure 2. The time-scales are normalized at $n_e T = 3 \times 10^{15}$ cm^{-3} K. The ionization time-scale is equal to $(n_e[C_{ea}(T) + C_{di}(T)])^{-1}$ where C_{ea} is the autoionization excitation rate coefficient (which is significantly large for the lithium-like ion O^{+5} and for iron ions in the sodium-sulphur series) and C_{di} is the direct (electron impact) ionization rate coefficient. The recombination time-scale is equal to $(n_e[\alpha_r(T) + \alpha_d(T)])^{-1}$ where α_r is the radiative recombination rate and α_d is the

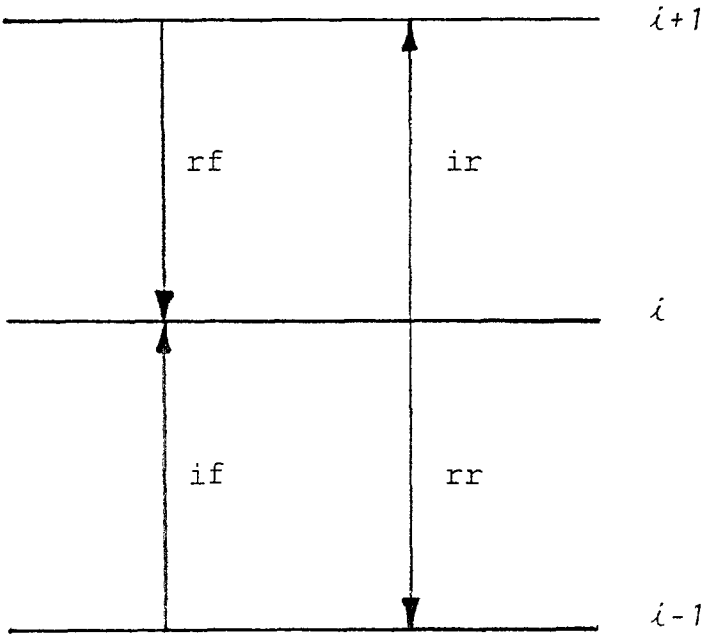

Fig. 2. Schematic illustration of the nomenclature used for labelling the formation and removal processes of species *i*.

dielectronic recombination rate. Table III contains results extracted from Table II for the temperature $T_{\max}$ at which a species attains its maximum abundance.

Normally the power emitted per unit volume in a single line by a plasma in equilibrium is written as the product of an emission rate coefficient, P_λ, and n_e^2. Note that even though in equilibrium plasmas the concentrations of species such as C^{+5} and Fe^{+9} may peak at the same temperature, the behavior of the line emissivities will differ greatly in response to rapid heating, as shown by the differences in the P_λ/f curves; this behavior during rapid heating was discussed at the beginning of Section 3.1. P_λ/f should be multiplied by the fraction of the element in the appropriate species to calculate the power in the line when the plasma is not in equilibrium.

Assume that we are interested in observing the emission from a species formed by the ionization of more lowly ionized species in a plasma which has been rapidly heated. The charge on the nucleus of that species is z and its ionization stage is ζ where $\zeta = 0$ for a neutral species and $\zeta = z$ for a fully ionized system. The number density is written $n_{z,\zeta}$. Because the ionization time-scale increases rapidly with charge, it is normally sufficient to assume that a large fraction of an element is initially in the next lowest ionization stage when calculating the evolution of the population of a species. During the interval when $n_{z,\zeta}$ peaks, the system of equations

$$\mathrm{d}n_{z,\zeta-1}/\mathrm{d}t = -n_{z,\zeta-1}/t^*_{if} + n_{z,\zeta}/t^*_{rr},$$

$$\mathrm{d}n_{z,\zeta}/\mathrm{d}t = n_{z,\zeta-1}/t^*_{if} + n_{z,\zeta+1}/t^*_{rf} - (1/t^*_{ir} + 1/t^*_{rr})n_{z,\zeta},$$

$$n_{z,\zeta+1} = n_z - n_{z,\zeta} - n_{z,\zeta-1},$$

$$n_{z,\zeta-1}(t=0) = n_z$$

TABLE III

Ionization and recombination time-scales[a] for selected lines

Ion	$\log(T_{max})$	$-\log(f)$	t_{if} (s)	t_{ir} (s)	t_{rf} (s)	t_{rr} (s)	τ_{app}
C^{+5}	6.0	0.2	120	1.1e3	290	270	65
Fe^{+23}	7.2	0.5	590	1.4e3	890	1.0e3	206
Fe^{+21}	7.0	0.7	260	460	220	200	75
Fe^{+17}	6.7	0.4	120	190	150	210	51
Fe^{+16}	6.4	0.1	23	1.4e3	130	21	10
Fe^{+15}	6.3	0.9	16	40	13	9.9	4.2
Fe^{+14}	6.3	0.8	9.0	16	9.9	7.0	2.8
Fe^{+13}	6.2	0.8	8.3	15	4.3	5.8	1.9
Fe^{+11}	6.2	0.6	2.4	4.6	3.9	3.9	1.1
Fe^{+10}	6.1	0.6	2.2	3.7	2.6	2.4	0.80
Fe^{+9}	6.0	0.6	2.0	3.5	1.6	1.4	0.54
Fe^{+8}	6.0	0.5	0.8	2.0	1.3	2.2	0.40
Mg^{+9}	6.1	0.7	21	69	200	56	14
Ne^{+7}	5.8	0.6	13	56	100	18	7.0
Ne^{+6}	5.7	0.5	4.0	29	11	3.3	1.6
O^{+7}	6.4	0.3	230	1.1e3	710	460	103
O^{+6}	6.3	0.3	0.4	480	390	420	0.4
O^{+5}	5.5	0.6	4.1	0.08	63	5.8	2.3
O^{+4}	5.4	0.3	0.8	10	3.7	1.1	0.4
Si^{+11}	6.3	0.6	42	130	290	95	26
Si^{+10}	6.2	0.6	21	74	60	18	8.3
Si^{+7}	5.9	0.3	4.9	19	7.8	10	2.3

[a] At the temperature of maximum emission.

will govern the behavior of $n_{z,\zeta}$. The asterisks on t_{if}^*, t_{rf}^*, t_{ir}^*, and t_{rr}^* indicate that they should be evaluated by multiplying the results in Table II by $(3 \times 10^{15}\ \mathrm{cm}^{-3}\ \mathrm{K}/n_e T)$. Values of P_λ/f can be used with the derived $n_{z,\zeta}$ to calculate the line strengths.

The abundance of a species $n_{z,\zeta}$ in a plasma which is heated can be approximated from the above equations if a few simplifying assumptions are made. We assume that initially $n_{z,\zeta-1} = n_z$, and throughout the initial rise in $n_{z,\zeta}$ that $n_{z,1}$ can be set to 0. The question we ask is, if the plasma is heated instantaneously to a higher temperature, what is the time-scale to form species z, ζ? Given these assumptions, one can show that

$$n_{z,\zeta} = (n_z \tau_{app}/t_{if}^*)\,(1 - e^{-t/\tau_{app}})$$

with

$$\tau_{app} = (t_{if}^{-1} + t_{ir}^{-1} + t_{rr}^{-1})^{-1}\,.$$

Values of this quantity for the species which we considered are given in Table III.

The abundance of a particular species in a recombining plasma cannot always be followed with such a small set of equations, because the recombination time-scale is not a strongly monotonically decreasing function of ζ. At $\log T = 6.5$ the values of t_{rr} for Fe^{+23}, Fe^{+21}, Fe^{+11}, and Fe^{+8} are 43.4 s, 27.8 s, 14.5 s, and 21.8 s, respectively. Hence, in a plasma which has cooled very rapidly, the recombination eventually leads

to significant populations in a range of ionization stages. However, in many cases it is sufficient to compare the recombination time-scales to the cooling time-scales to determine at what temperature the ionization structure is last in statistical equilibrium. As long as the recombination continues to occur on a time-scale long compared to either the cooling time-scale or the time-scale since rapid cooling gas stopped, the ionization structure can be assumed to be that which obtained in an equilibrium plasma at the temperature at which cooling first becomes more rapid than recombination.

The set of equations given above should be sufficient to follow the abundance of a species z, ζ in a cooling plasma under certain restricted conditions. For instance, if a plasma is cooling from an equilibrium at which $n_{z,\zeta} \gg n_{z,\zeta+i}$ for all $i > 2$, the three equations should give a reasonable description of the evolution of $n_{z,\zeta}$. Clearly, the initial values of $n_{z,\zeta-1}$, $n_{z,\zeta}$, and $n_{z,1}$ should be specified to be those for a plasma in equilibrium at the initial temperature.

We have given in Table IV the time-scales for cooling due to radiative losses in equilibrium plasma in which $n_e T = 3 \times 10^{15}\ \mathrm{cm}^{-3}\ \mathrm{K}$ initially; these time-scales are appropriate for a plasma cooling isochorically and were obtained by using data given in a figure produced by R. Edgar with J. Raymond's code and provided by J. Raymond, showing the power loss coefficient as a function of temperature. The cooling time-scale for isobaric cooling is obtained by multiplying the results given in Table IV by $\frac{5}{3}$.

The time-scale for conductive cooling may be calculated by considering a loop of half-length l in which radiative losses are balanced exactly by heating and which is cooling isochorically due to conduction. Several approximate solutions have been calculated for this case; Krall (1977) has suggested that the temperature, T_0, at the apex of the loop evolves as

TABLE IV

Radiative cooling time-scales for an equilibrium plasma

$\log T$	t_{cool} (s)	n_e [a]	$\log T$	t_{cool} (s)	n_e [a]
4.8	0.87	5.0e10	6.1	690	2.4e9
4.9	0.97	4.0e10	6.2	970	1.9e9
5.0	1.5	3.0e10	6.3	2.2e3	1.5e9
5.1	3.9	2.4e10	6.4	5.5e3	1.2e9
5.2	5.5	1.9e10	6.5	1.4e4	1.0e9
5.3	7.7	1.5e10	6.6	1.9e4	8.0e8
5.4	11	1.2e10	6.7	3.1e4	6.0e8
5.5	27	1.0e10	6.8	4.9e4	5.0e8
5.6	69	8.0e9	6.9	7.8e4	4.0e8
5.7	140	6.0e9	7.0	1.1e5	3.0e8
5.8	220	5.0e9	7.1	2.2e5	2.4e8
5.9	340	4.0e9	7.2	4.4e5	1.9e8
6.0	490	3.0e9	7.3	8.5e5	1.5e8

[a] Assuming solar abundances and $n_e T = 3 \times 10^{15}\ \mathrm{cm}^{-3}\ \mathrm{K}$. Cooling is assumed to occur isochorically; time-scales for isobaric cooling are obtained by multiplying these values by $\frac{5}{3}$.

$$T_0 = T_{00}\left(1 + \frac{1.4 \times 10^9 T_{00}^{5/2} t}{nl^2}\right)^{-2/5},$$

where T_{00} is the initial temperature at the apex of the loop.

In calculating the conductive cooling time we will use Krall's result. However, we note that the equation of thermal balance is a partial differential equation with time and spatial derivatives; if one assumes that conductivity is the only process responsible for energy loss or gain, that flows are very subsonic, that the loop is a cylinder in which conductive heat transfer is parallel to the axis of symmetry, and that the gas cools either isobarically or isochorically, then the equations can be solved by a separation of variables. No such solution exists for a cooling loop with $T = 0$ at the base and T a maximum at the top. Consequently, any value for the conductive cooling time which one may adopt is somewhat arbitrary and is likely to be correct only to within an order of magnitude of the true value.

3.3. Emission from solar coronal features

We have given in Table V typical time-scales for the appearance and disappearance of lines prominent in the spectra of the coronal features listed in Table Ib, using the temperature and density values appropriate to the different types of regions under consideration. The time-scales given take into account the number, $n_{z,\zeta}$ of atoms contributing to the emission and are calculated in several steps. τ_{app}, the minimum time for the appearance of the line, is the ionization time for formation of $\sim 60\%$ (one e-folding) of the ion from the next less ionized state of the element, calculated assuming the temperature instantaneously becomes the maximum temperature for emission of the line. These times were calculated from the times listed in Table III using the tempera-

TABLE V

Heating and cooling time-scales[a] for solar coronal features

Feature	Line	τ_{app}	τ_{recom}	$\tau_{dis,\,cond}$	$\tau_{dis,\,rad}$
Quiet corona	O VII	3.0	$3 + 10^3$	5×10^4	10^4
Extended corona	Fe X	120	500	2×10^4	1.5×10^5
	Mg X	2000	4×10^4	2×10^4	1.5×10^5
Polar plumes	Fe X	12	50	10^5	1.4×10^4
	Mg X	370	4.5×10^3	10^5	1.4×10^4
Active region	O VIII	28	200	8×10^4	10^3
	Fe XVII	4.0	30	10^5	10^3
Microstructure	Fe XVIII	1.0	1.2	600	600
	Fe XXII	3.0	0.7	250	400
X-ray bright point	O VII	0.1	100	800	500
Compact flare	Fe XXII	3.0	1.3	400	10^3
	Fe XXIV	10	2	750	2×10^3
Two-ribbon flare	Fe XVIII	5.0	6	10^4	3×10^3
	Fe XXII	15	3	5×10^3	2×10^3

[a] Using T and n_e values from Table Ib. All times are in seconds.

tures and pressures typically found in the coronal features emitting the line. τ_{recom} is a lower limit on the disappearance time of the line. It is the time for 60% of the ion to recombine to the next less ionized state at the temperature and pressure found in the coronal feature.

For comparison also given is $\tau_{dis,\,cond}$, the disappearance time-scale of the line assuming that conductive cooling is the dominant cooling mechanism, and $\tau_{dis,\,rad}$, the disappearance time-scale of the line assuming that radiative cooling is the dominant cooling mechanism. In order to maintain consistency with the method used to calculate time-scales for the appearance of a line, we have calculated the times for the temperature to drop sufficiently to cause emissivity of the line to drop to $1/e$ of its maximum value. Conductive cooling rates were calculated assuming constant heat flux throughout the loops (Krall, 1977). Radiative cooling rates were calculated using analytic fits to Raymond's power loss function (viz., Rosner, Tucker, and Vaiana, 1978).

$\tau_{dis,\,cond}$ and $\tau_{dis,\,rad}$ were calculated assuming ionization equilibrium. In these cases, it is necessary to consider not only the time-scale for a given change in temperature which is given directly from the cooling curves, but also to consider the change in emission which occurs for a given change in temperature. In this way, the time-scales given in Table V for disappearance of a line refer to the same quantities listed for appearance of the line.

The cooling time-scale due to radiative losses is inversely proportional to the pressure, in optically thin plasmas. For the high temperature plasmas encountered in active regions and flares in the solar corona, the pressures are usually very much higher than the value of 3×10^{15} which we have used as a normalization. Thus radiative cooling times for flares are typically 10^2 to 10^3 s and are comparable to the typical conductive cooling times calculated for flare loops. We wish to point out only that conductive cooling may in some cases be more important than radiative cooling in the coronal plasma. As discussed above, freezing-in can occur when the cooling is very rapid, and in those cases simultaneous observations of properly chosen high- and low-excitation lines should be used in order to diagnose both the emission measure and the temperature variations.

3.4. The case of Mg X

Of the lines listed in Table V, the only one for which freezing-in might occur under coronal conditions is Mg X emitted by large-scale coronal structures. However, as pointed out in Section 3.3, the correct values for conductive cooling times are uncertain by a large factor and conductive cooling might be important in a wider variety of situations in the solar atmosphere; the opposite may also be true. Under the assumption that there will turn out to be cases for which we need to consider rapid cooling we give a treatment which is of general validity for a gas which has just begun to cool isochorically.

The total power emitted in a line in a cooling plasma is given by

$$E_\lambda(z, \zeta) = P_\lambda(z, \zeta) X(z, \zeta) (n_e^2 V),$$

where $P_\lambda(z, \zeta)$ is the line power rate coefficient, V is the volume of the emitting gas, λ is the wavelength, and

$$X(z, \zeta) \equiv n_{z,\zeta}/n_e .$$

In general, the mass of gas will remain constant as it cools, i.e., $n_e V$ remains constant. We restrict consideration to rapid cooling so that n_e remains constant; this is equivalent to requiring that the sound crossing time in the loop is long compared to the cooling time. The time-scale on which the line strength varies is then given by

$$t_{\text{dis}} = \left(P_\lambda^{-1} \frac{dP_\lambda}{dT} \, dT/dt + X^{-1} \, dX/dt \right)^{-1} .$$

A reasonable estimate for t_{dis} is obtained by replacing dT/dt with

$$(T/t_{\text{rad}} + T/t_{\text{cond}})$$

and $X^{-1} \, dX/dt$ with the minimum of

$$\left[\frac{1}{X_{\text{eq}}(z, \zeta)} \frac{dX_{\text{eq}}(z, \zeta)}{dT} \left(\frac{T}{t_{\text{rad, cool}}} + \frac{T}{t_{\text{cond, cool}}} \right), \frac{1}{t_{rr}^*} \right],$$

where X_{eq} is given from equilibrium calculations.

The data necessary to calculate t_{dis} for Mg X are given in Table II and IV, and by the equation for the conductive cooling time. If the Mg^{+9} abundance freezes-in then observations of Mg X at, for example, both 63 and 609 Å will permit a determination of the temperature over a broader range than if the Mg^{+9} attained its equilibrium value. This also means that the time-scale for disappearance of the Mg X emission can be significantly larger than that of another ion formed at a similar temperature. Under conditions of rapid cooling (which presumably alternate with periods of heating) the 609 Å line will show less variability than will the 63 Å line. Measurement of both lines permits an accurate temperature determination, and measurement of a line of a species which attains equilibrium abundance rapidly (such as O VII) can be used to determine the emission measure and thence n_e.

4. Summary

With a view toward observations of the solar transition region and corona using imaging of individual spectral lines in the soft X-ray and XUV portion of the spectrum, we have discussed some of the major factors which enter into the choice of spectral line to be used. The discussion has centered around the lines which are available to the technology of multilayer coatings, but is more general in its range of applicability. Because of our interest in coronal heating and the rapid variability of coronal structures we have concentrated on the observability of variations in line strength for the range of features found in the solar corona. Examination of the ionization and recombination time-scales for the formation and removal of ions which are prominent in the coronal spectrum

shows that variability time-scales are often limited by these atomic processes, independent of the physical process which might be assumed to be causing the changes.

In some situations, the plasma may be heated on time-scales which are short compared to the time needed for the ionization structure to attain equilibrium. Such rapid heating can lead to a freezing-in of the initial ionization structure. In such cases, comparison of a low excitation line of a species to a high excitation line (preferably of the same species) would permit accurate determination of the time evolution of both the emission measure and the temperature. Similarly, there are some situations in which rapid cooling may lead to a freezing-in of the abundance of an ion. In particular, Mg X viewed in large-scale coronal structures should show this effect. Observations in the 609 Å line of Mg X should be supplemented by a short wavelength line such as Mg X at 63 Å.

Studies of rapid variability in active regions should be performed with spectral lines which are capable of being formed on short time-scales. For example, at typical active region temperatures of $2–3 \times 10^6$ K, the species O VII can appear on times a factor 100 shorter than those for the appearance of O VIII. Disappearance times for O VII are about one order of magnitude shorter than those for O VIII.

Acknowledgements

This work was supported by NASA Grant NAGW-112 to the Smithsonian Institution and by the Smithsonian Institution Visitors' Program. We would like to thank Dr. John Raymond for helpful discussions during preparation of this manuscript.

References

Acton, L. W., Bruner, M. E., and Brown, W. A.: 1985, *Astrophys. J.* **291**, 865.
Arnaud, M. and Rothenflug, R.: 1985, *Astron. Astrophys. Suppl. Ser.* **60**, 425.
Barbee, T. W.: 1985, *SPIE Proc.* **563**, 2.
Catura, R. C. and Golub, L.: 1988, *Rev. Phys. Appl.* **23**, 1741.
Doschek, G. A. and Cowan, R. D.: 1984, *Astrophys. J. Suppl. Ser.* **56**, 67.
Freeman, F. F. and Jones, B. B.: 1970, *Solar Phys.* **15**, 288.
Golub, L., Nystrom, G., Spiller, E., and Wilczynski, J.: 1985, *SPIE Proc.* **563**, 266.
Krall, K. R.: 1977, *Solar Phys.* **55**, 455.
Kuperus, M., Ionson, J. A., and Spicer, D. S.: 1981, *Ann. Rev. Astron. Astrophys.* **19**, 7.
Malinovsky, M. and Heroux, L.: 1973, *Astrophys. J.* **181**, 1009.
Manson, J. E.: 1972, *Solar Phys.* **27**, 107.
Martens, P. C. H., van den Oord, G. H. J., and Hoyng, P.: 1985, *Solar Phys.* **96**, 253.
Mewe, R., Gronenschild, E. H. B. M., and van den Oord, G. H. J.: 1985, *Astron. Astrophys. Suppl. Ser.* **62**, 197.
Nolte, J. T., Solodyna, C. V., and Gerassimenko, M.: 1979, *Solar Phys.* **63**, 113.
Rosner, R., Tucker, W. H., and Vaiana, G. S.: 1978, *Astrophys. J.* **220**, 643.
Shapiro, P. R. and Knight, J. W.: 1978, *Astrophys. J.* **224**, 1028.
Shapiro, P. R. and Moore, R. T.: 1977, *Astrophys. J.* **217**, 621.
Sheeley, N. R., Jr. and Golub, L.: 1979, *Solar Phys.* **63**, 119.
Shull, J. M. and Van Steenberg, M.: 1982, *Astrophys. J. Suppl. Ser.* **48**, 95.
Stem, R., Wang, E., and Bowyer, S.: 1978, *Astrophys. J. Suppl. Ser.* **37**, 195.
Underwood, J. H., Bruner, M. E., Haisch, B. M., Brown, W. A., and Acton, L. W.: 1987, *Science* **238**, 61.
Walker, A. B. C., Lindblom, J., Hoover, R. B., and Barbee, T. W.: 1989, *Proc. IAU Colloq.* No. 102 (in press).
Woods, D. T., Shull, J. M., and Sarazin, C. L.: 1981, *Astrophys. J.* **249**, 399.